

Alcohol-free synthesis, biological assessment, in vivo toxicological evaluation, and in silico analysis of novel silane quaternary ammonium compounds differing in structure and chain length as promising disinfectants

Ghada Tagorti ^a, Burçin Yalçın ^a, Merve Güneş ^a, Ayşen Yağmur Burgazlı ^a, Tuğçe Kuruca ^b, Neslihan Cihanoğlu ^b, Esin Akarsu ^b, Nuray Kaya ^a, Ricard Marcos ^{c,*}, Bülent Kaya ^{a,*}

^a Department of Biology, Akdeniz University, Antalya, Turkey

^b Department of Chemistry, Akdeniz University, Antalya, Turkey

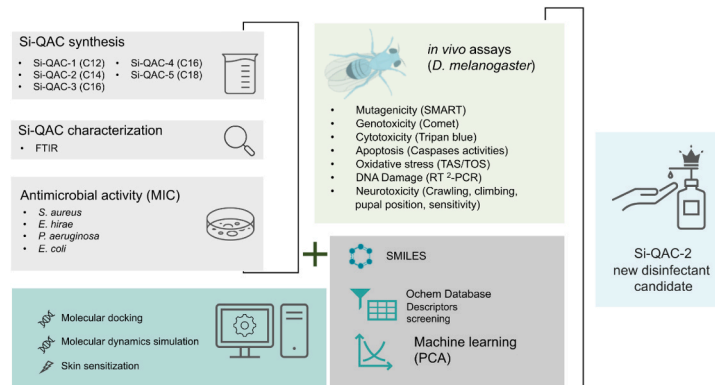
^c Department of Genetics and Microbiology, Universitat Autònoma de Barcelona, Cerdanyola del Vallès, Spain



HIGHLIGHTS

- New silane quaternary ammonium disinfectants were synthesized.
- The antimicrobial effect depends on alkyl chain length and the presence of silane.
- Mutagenicity/genotoxicity were observed on low alkyl chain compounds.
- From in vivo/in silico data one compound (Si-QAC2) was selected as a promising disinfectant.
- In silico data detect crucial descriptors to guarantee the safety of Si-QAC.

GRAPHICAL ABSTRACT



ARTICLE INFO

Lingxin CHEN

Keywords:
DNA damage
Drosophila melanogaster
Genotoxicity
Oxidative stress

ABSTRACT

Quaternary ammonium compounds (QACs) are commonly used as disinfectants for industrial, medical, and residential applications. However, adverse health outcomes have been reported. Therefore, biocompatible disinfectants must be developed to reduce these adverse effects. In this context, QACs with various alkyl chain lengths (C12–C18) were synthesized by reacting QACs with the counterion silane. The antimicrobial activities of the novel compounds against four strains of microorganisms were assessed. Several in vivo assays were conducted on *Drosophila melanogaster* to determine the toxicological outcomes of Si-QACs, followed by computational analyses (molecular docking, simulation, and prediction of skin sensitization). The in vivo results were combined using a cheminformatics approach to understand the descriptors responsible for the safety of Si-QAC. Si-QAC-2 was active against all tested bacteria, with minimal inhibitory concentrations ranging from 13.65 to 436.74 ppm. *Drosophila* exposed to Si-QAC-2 have moderate-to-low toxicological outcomes. The molecular

* Corresponding authors.

E-mail addresses: ricard.marcos@uab.es (R. Marcos), bkaya@akdeniz.edu.tr (B. Kaya).

weight, hydrophobicity/lipophilicity, and electron diffraction properties were identified as crucial descriptors for ensuring the safety of the Si-QACs. Furthermore, Si-QAC-2 exhibited good stability and notable antiviral potential with no signs of skin sensitization. Overall, Si-QAC-2 (C14) has the potential to be a novel disinfectant.

1. Introduction

Over the past few decades, quaternary ammonium compounds (QACs) have been widely used as effective disinfectants. This is because of their unique mode of action: interacting with the bacterial cell membrane, which exhibits a negative electrostatic potential, and QAC nitrogen molecules, which have a positive charge, leading to membrane disruption and cell death [47].

QACs are widely used in diverse environments, including hospitals, care facilities, and workplaces [66]. However, the onset of the recent pandemic has increased QAC consumption, which is potentially detrimental to human health due to the reported harmful effects [11,16,44]. For instance, it has been demonstrated that QACs can lead to respiratory tract inflammation, dry skin, asthma, and chronic obstructive pulmonary disease [11]. Therefore, QACs are considered environmental compounds of special health concern.

Moreover, QACs are subject to incomplete elimination during the wastewater treatment process and can, therefore, be discharged into the ecosystem [46]. This can increase the risk of antibiotic resistance [8]. Because QAC degradation processes in the environment are limited, it is anticipated that QACs will have extensive ecotoxicological repercussions, such as toxicity to aquatic organisms [4]. Eco-friendly and biocompatible disinfectants have been proposed as alternatives to ensure ecosystem safety.

Substantial advancements have recently been made in response to the COVID-19 pandemic, aiming to develop effective disinfectants [13, 2,63]. Nevertheless, the shortcut of fundamental materials such as alcohol remains a significant issue that needs to be adequately addressed. Furthermore, avoiding bacterial resistance and maintaining human and environmental safety profiles are crucial issues that should be addressed [64]. To overcome these challenges, a recent study scrutinized nine distinct QACs, characterized by variable chain lengths and counterions, to evaluate their efficacy in mitigating adhesion across diverse surfaces [33]. However, the counterion silane was not evaluated. Unlike previous studies, our current research uses a singular counterion known as the silane group. This selection introduces a novel dimension to the study as the impact of silane as a counterion is considered an undiscovered subject. Therefore, a group of novel alcohol-free, synthetic disinfectants based on silane groups (Si-) and QACs with alkyl chains of variable lengths (C12, C14, C16, and C18) were synthesized and characterized in the present study.

To ensure the safety of the newly synthesized compounds, a wide set of assays was conducted to determine their potential hazards. First, the antimicrobial activities of the synthesized compounds were evaluated. Considering the potential uses of these novel compounds, various toxicological endpoints were assessed in *Drosophila melanogaster*, a well-known *in vivo* model organism. Molecular docking is a valuable method for predicting the interactions between small molecules and target macromolecules to gain insights into biological processes and identify potential drug candidates [50,54]. Additionally, machine learning and data analysis have been used to develop more accurate models to predict the antiviral potential of compounds and to accelerate the discovery of effective antimicrobial therapeutic candidates [31,36]. Given the potential of these tools, *in silico* analyses, including molecular docking and machine learning (principal component analysis), were performed to elucidate the properties of Si-QACs better.

2. Materials and methods

2.1. Chemicals

All chemicals used for the present study are listed in Table S1 (Supplementary Materials).

2.2. Bacterial strains

Four different strains of bacteria were used according to the instruction of Biocidal Product Analysis and Authorized Laboratories for the medical, public, and personal workspaces determined by the General Directorate of Public Health of Türkiye (TS EN 1276, TS EN 13727 +A2, TS EN 1650, TS EN 13624). The strains are two Gram (+): *Staphylococcus aureus* (ATCC 6538), *Enterococcus hirae* (ATCC 10541), and two Gram (-): *Escherichia coli* (ATCC 10536), *Pseudomonas aeruginosa* (ATCC 15442).

2.3. Si-QACs synthesis and characterization

Each QAC compound and (3-chloro propyl)trimethoxysilane were fed in equal proportions into a pressure reactor under an argon atmosphere at 130 °C for 72 h. Once the reaction was complete, the final solution was collected as yellow-colored viscous liquids. The process parameters of the Si-QACs synthesis are listed in Table S2 (Supplementary materials).

The FTIR spectra of each synthesized Si-QACs were recorded on a PerkinElmer Frontier spectrometer with spectra over the 4000–500 cm⁻¹ region, with a resolution of 4 cm⁻¹. The Spectrum software (Perkin-Elmer LLC 1500F2429, v5.0.1) was used to calculate the data from the spectra.

2.4. Minimal inhibitory concentration (MIC)

The antimicrobial efficacy was evaluated using the microdilution method, according to Clinical and Laboratory Standards Institute (CLSI) recommendations. Benzalkonium chloride (BAC), a commercially available quaternary ammonium compound used as a disinfectant, was used as a positive control, and screened against all bacterial strains. The assay was performed in 96 well plates using stocks of five Si-QACs dissolved in distilled water. Concentrations from 16 to 1024 ppm were analyzed. Bacterial suspensions were prepared in Mueller-Hinton broth (10⁶ CFU/mL). To maintain the same concentration of viable strains, they were administered the last. First, 100 µL per well of each Si-QAC was added to serial two-fold dilutions. Later, 100 µL of broth was added to each well (5 × 10⁶ CFU/mL) and incubated for 48 h at 37 °C. The MIC was defined as the lowest biocide concentration completely inhibiting bacterial growth, which was determined after visual inspection. Three independent replicates were performed.

2.5. Fly strains and stock maintenance

Two strains of *D. melanogaster* were used in the wing Somatic Mutation and Recombination Test (SMART): (i) multiple wing hairs (*mwh/mwh*), and (ii) flare-3 (*flr³/In(3LR)TM3, ri p^B sep l(3)89Aa bx34^c Bd^d*). The wild-type *Drosophila*, Oregon R+, was used in the remained assays. Flies were reared in a standard cornmeal-based medium in glass vials and housed in incubators at 60% humidity, and a temperature of nearly 25 ± 1 °C, on a 12:12 h light/dark daily cycle.

2.6. Si-QACs exposure

Drosophila flies were exposed to Si-QACs via ingestion through the instant medium (Blue formula, Ward's science, US) wetted with the selected concentration of the Si-QACs. The synthesized Si-QACs were dissolved in distilled water. The concentration at which the growth of the bacteria strains was inhibited corresponds to the reference concentration (100%) of that specific Si-QAC. Thus, the maximum concentration was considered as 2-fold the reference concentration (300%), and one-fourth of the reference concentration (25%) was pointed as the lowest used concentration. In this sense, five concentrations (25%, 50%, 100%, 200%, and 300%) for each Si-QAC were set up for the survival test (Table 1).

Distilled water was used as a negative control for all experiments, and phosphate-buffered saline (PBS) was included as a negative control solely in the caspase activities measurement assay. Ethyl methanesulfonate (EMS), an alkylating chemical, is a Group 2B agent by the International Agency for Research on Cancer (IARC), meaning the compound could be a possible carcinogenic to humans due to the conversion of the GC pair into AT pair and vice versa [20]. This compound was used as a positive control at 1 mM and 4 mM concentrations for SMART and comet assay respectively according to our previous studies [21,58]. Hydrogen peroxide (H₂O₂) induced oxidative stress in *Drosophila* [28], and reduced the survival of flies at 0.05 M according to our previous studies (unpublished data). Therefore, H₂O₂ (0.05 M) was selected as a positive control for the trypan blue assay.

For all experiments, third-instar larvae (72 ± 4 h old) were collected from the standard medium and transferred to plastic vials containing 1.5 g of instant medium wetted with 9 mL of each Si-QAC with the selected concentration based on survival assay. Chronic exposure was conducted, and three replicates were performed.

2.7. Survival assay

Fifty third-instar larvae were reared in each experimental condition. The number of emerging adult flies was counted. The mortality percentages were subjected to *aomisc* (sigmoid curve) and *nlstools* packages analysis [6] using RStudio (RStudio [52]) to estimate the lethal concentrations.

2.8. Biomarkers

2.8.1. Mutagenicity

The SMART assay was used to determine the mutagenic (deletion, point mutation, and non-disjunction), recombinogenic, and anti-genotoxic potential of chemical compounds [57]. A standard cross between *mwh* males and virgin *fltr*³ females was conducted to produce two progenies: (i) trans-heterozygous (*mwh/fltr*³) with normal wings and balancer heterozygous (*mwh/TM3, Bd*⁵) with serrated wings. From this cross, eggs were collected for 8 h in glass vials with the standard medium. Third-instar larvae (72 ± 4 h old) were collected and transferred to vials containing experimental medium to chronic treatment (approximately 48 h). The experimental medium is composed of 1.5 g of instant medium hydrated with 9 mL of experimental solution. Emerging flies were collected and stored in 70% ethanol at 4 °C. The wings of

Table 1
The Si-QAC concentrations used in the survival assay.

Compound	25% Concentration in ppm	50%	100%	200%	300%
Si-QAC-1	28.16	56.32	112.64	225.28	337.92
Si-QAC-2	109.18	218.37	436.74	873.48	1310.22
Si-QAC-3	7.20	14.40	28.80	57.60	86.40
Si-QAC-4	15.75	31.50	63.00	126.00	189.00
Si-QAC-5	12.75	25.50	51.00	102.00	153.00

trans-heterozygous flies were removed with the aid of forceps on a stereomicroscope and mounted on glass slides using Faure's solution (30 g gum Arabic, 50 g chloral hydrate, 20 mL glycerol, 50 mL distilled water). The coverslip to the slides was conducted using Faure's solution and metal weight (~ 200 g). Both dorsal and ventral surfaces of the wings were analyzed for the frequency of spots under an optical light microscope (Nikon-YS100; Nikon Co., Tokyo, Japan) at 400x magnification. Mutant spots were classified as follows: (i) small single spots (1–2 cells in size with *mwh* type), (ii) large single spots (≥ 2 cells in size with *mwh* type or ≥ 4 cells in size with *fltr*³ type), and (iii) twin spots (*mwh* and *fltr*³ cells are in the same area with less than 2) [37].

2.8.2. Genotoxicity

The alkaline version of the comet assay was performed as described aiming to assess DNA strand breaks (DSB) production [37]. Larvae (n = 60/ experimental condition) were embedded in a mixture solution (0.07% N-phenylthiourea dissolved in PBS) and their cuticles were ruptured with the aid of forceps. The hemolymph was collected and centrifuged (300 ×g, 10 min, 4 °C) to be suspended in LMA (100 µL sample: 80 µL of 0.75% LMA). The homogenate was layered onto slides pre-coated with 1% NMA, covered with coverslips, and cooled on ice for 15 min until agar solidification. Next, coverslips were removed, and the same procedure of LMA-coating and cooling was repeated. Slides were immersed into freshly prepared lysis solution (2.5 M NaCl, 100 mM Na₂EDTA, 10 mM Tris, 1% Triton X-100%, and 1% N-lauroylsarcosinate, pH=10) for 1 h at 4 °C in a dark environment. The next steps were performed under dim light to avoid any supplemental DNA damage.

After lysis, slides were transferred to a horizontal gel-electrophoresis tank filled with buffer (1 mM Na₂EDTA, 300 mM NaOH, pH = 13) for 30 min followed by electrophoresis (300 mA, 25 V, 30 min). Slides were washed twice in Tris-buffer (400 mM; pH=7.5), followed by distilled water, and then dried. Later, slides were stained with ethidium bromide (at 60 µg/mL), covered with a coverslip, and incubated for 20 min at 4 °C. The cell analysis was conducted at 400x magnification using a fluorescence microscope (Nikon Eclipse E200, Germany) with $\lambda = 480$ –550 nm excitation filter and $\lambda = 590$ nm barrier filter and was scored using Comet Assay IV™ software (version 4.11; Perceptive Instruments, Suffolk, UK), computing the tail intensity (%DNA in the tail) from 50 comets per experimental condition as a measure of DNA damage.

2.8.3. Cytotoxicity

The trypan blue assay was conducted to determine midgut damage in *Drosophila*. Ten larvae (96 ± 4 h old) were randomly collected from the experimental vials and cleaned with PBS (1 ×/2 min) to eliminate the residual medium. Larvae were later relocated to a Petri dish containing a trypan blue solution (0.2%) and incubated for 40 min at room temperature. Afterward, larvae were washed twice with PBS (1 ×/7 min) to remove any trace of blue color present on their body surface. Larvae were transferred with a brush to glass slides to score midgut damage under a stereomicroscope. The degree of damage was classified into five categories: (0) no blue color, no damage; (1) blue-colored dot, minor damage; (2) two blue-colored dots, moderate damage; (3) approximately half of the midgut is blue-colored, major damage; and (4) blue-dark-colored midgut, extreme damage.

2.8.4. Oxidative stress

Total antioxidant status (TAS, mmol Trolox Eq/L) and total oxidant status (TOS, µmol H₂O₂ Eq/L) were measured as published [14]. Thirty larvae (96 ± 4 h old) were collected from each experimental condition, transferred to micro-centrifuge tubes supplemented with PBS (1 mL/tube) to be grounded using a ball mill (Retsch MM 400, Retsch GmbH, Germany), followed by centrifugation (1500 ×g, 10 min, 4 °C). TAS and TOS were calculated as per the manufacturer's recommendations (Real Assay Diagnostics, Türkiye). The oxidative stress index (OSI) was calculated as the ratio TOS/TAS.

2.8.5. Apoptosis

Caspase activities measurement was set up based on a previous method [15]. Third-instar larvae hemocytes exposed to Si-QACs at different concentrations were isolated according to a previously described method [27]. The collected hemocytes were treated for 1 h at 4 °C with lysis solution (150 mM NaCl, 2 mM Na₂EDTA, 20 mM Tris, 1% Triton X-100, 2.5 mM sodium pyrophosphate, and 1 mM β-glycerophosphate). Later, treated hemocytes were centrifuged (1500×g, 15 min, 4 °C) and the supernatant was used to perform the bicinchoninic acid assay to maintain the same level of proteins in each sample (100 µg protein/100 µL). Caspase-Glo 3/7, 8, and 9 reagents (Promega, Madison, WI, USA) were transferred with the samples (ratio 1:1) to a 96-well plate to be incubated for 1 h at room temperature. The luminescence was measured using GloMax-Multi Microplate Multimode Reader (Promega).

2.8.6. DNA repair efficiency

A custom gene array panel was generated to analyze the DNA damage and repair mechanisms after exposure to xenobiotics [21,65]. In the current study, the RT² Profiler *Drosophila* DNA Damage Signaling Pathway PCR Arrays (CAPD14014, Qiagen) were used. This signaling pathway-focused array consisted of 36 genes related to DNA repair in *Drosophila*. Additionally, five housekeeping genes (reference) and panel controls including genomic DNA contamination (GDC), real-time PCR efficiency (PPC), and first-strand synthesis (RTC) were used. The use of this panel required RNA extraction, cDNA synthesis, PCR amplification, and gene expression analysis, as described below. All the reaction conditions and protocols were conducted according to the manufacturer's instructions.

• RNA extraction and cDNA synthesis

Thirty larvae (96 ± 4 h old) were collected from the highest (300%) and lowest (25%) concentration of each Si-QAC and grounded using a ball mill (Retsch MM 400, Retsch GmbH, Germany). The TissueLyser protocol was used to ensure the homogenization of larval tissues. RNA was isolated using RNeasy Mini Kit (CN: 74104, Qiagen). The obtained RNA was quantified using a NanoDrop spectrophotometer (ND-1000 Spectrophotometer V3.7, Thermo Fisher Scientific). For highly pure RNA, the 260/280 absorption ratio was ~2 and the 260/230 ratio was > 1.7. cDNA synthesis was performed using the RT² First Strand Kit (CN: 330404, Qiagen).

• PCR array plates

A custom RT²-PCR was conducted using RT² SYBR Green ROX qPCR Mastermix (CN:330523, Qiagen). Thermal cycling was performed on a Step-One Plus RT-PCR thermal cycler (Applied Biosystems) with the following cycle parameters: one cycle at 95 °C for 10 min, followed by 40 cycles at 95 °C for 15 s and 60 °C for 60 s. The cycle threshold (CT) values were exported as Excel files to the GeneGlobe Data Analysis Center (Qiagen) for further analysis.

2.8.7. Neurotoxicity

2.8.7.1. Pupal positioning. Fifty third-instar larvae were collected from the standard medium to be placed in the tested vials supplemented with experimental medium and divided into four sections: (1) the section above 1 cm from the top, (2) up to 1 cm from the medium, (3) nearly above the medium, (4) inside the medium. The number of pupae appearing in each of the sections was recorded.

2.8.7.2. Climbing assay. The climbing assay was performed according to a previously described method [19]. From each experimental condition, 30 flies (4 days old) were transferred after anesthesia using ether at room temperature into 15 cm length empty vials with a 10 cm mark from the bottom. A recovery period of 4 h was set to regain mobility and

coordination. Later, the vials were gently tapped to knock all flies to the bottom and the number of flies that climbed beyond the 10 cm mark was counted after 10 s

2.8.7.3. Crawling assay. Forty-five larvae (96 ± 4 h old) were retrieved from each experimental condition and gently washed in PBS (1x/ 2 min) to eliminate residual food medium. The crawling space consisted of a 12 cm² petri dish filled with 2% solidified agarose, placed over graph paper. Five larvae were transferred with a brush to the crawling space and allowed to adapt to the new environment. Later, larvae were placed in the center of the crawling space to allow free crawling for 1 min. A trailing impression was left by larvae once crawling on the agar gel, thus, with a marker the crawling path was sketched. The average crawling distance per minute was calculated [12].

2.8.7.4. Thermal sensitivity assay. The thermal sensitivity assay was conducted following a previous study [39]. Fifteen larvae (96 ± 4 h old) were collected from each condition after PBS wash (1x/ 2 min) to be placed in a Petri dish containing 2% solidified agarose at room temperature. The Petri dish was rubbed into parafilm to avoid humidity increase. Later the Petri dish was floated inside a tank filled with 200 mL of distilled water with a temperature ranging between 40–45 °C. After a 5-min adjustment period, the number of larvae that started to climb the lid of the Petri dish following the next 5 min was counted.

2.8.7.5. Cold sensitivity assay. Larvae were collected and prepared similarly to the protocol of the thermal sensitivity assay. The Petri dish was floated inside a tank filled with cold distilled water (14–18 °C). After 5 min acclimatization period, larvae behavior was observed for the following 5 min. Only larvae that hesitated to crawl were counted [39].

2.9. *in silico* analysis

SMILES and the structural MOL files of the synthesized Si-QACs have been created using ChemDraw and were further used to perform molecular docking and dynamics simulation, predict skin sensitization, and compute molecular descriptors.

2.9.1. Molecular docking

Open Babel (version 3.1.1) was used to convert MOL files to PDB files, a recommended format for AutoDock Tools (O'Boyle et al., 2011). The B-DNA (PDB ID:1BNA), Angiotensin Converting Enzyme 2 (ACE-2) in SARS-CoV-2 virus (PDB ID: 6M17), Capsid protein Hexon in Human adenovirus type 5 (PDB ID: 6CGV), and RNA-directed RNA polymerase (RdRp) in Influenza strain H5N1 (PDB ID: 6QPF) structures were retrieved from the protein data bank. Water and heteroatoms were removed, whereas polar hydrogen and charges were allocated to ligands and receptors using AutoDock Tools (version 1.5.6). The Si atom (Silicon) is not incorporated into the library parameter of AutoDock. Thus, a customized AD4 parameter file with all Si atom information was included. A grid box was generated, and docking was conducted using AutoDock 4 with all parameters deemed default. The best-docked structures with the lowest binding affinity were selected. BIOVIA Discovery Studio was used to analyze and visualize the structures (BIOVIA, 2021).

2.9.2. Molecular dynamics simulation

Molecular dynamics simulation of DNA-(Si-QAC) complexes was performed by using the iMODS server (<http://imods.chaconlab.org/>; accessed on 20 August 2023). The motion and structural flexibility of the docked complex were calculated by iMODS based on the normal mode analysis (NMA) [35]. The stability of the docked complex was depicted regarding its structural equilibria revealed via B-factors, deformability through marking the non-rigid section of the docked structure, eigenvalues, covariance matrix, and elastic network model. The input files

were docked structures with the lowest binding affinity saved as the PDB format, and uploaded to the server, with all parameters set to default.

2.9.3. Skin sensitization

Pred-Skin v3.0 (<http://predskin.labmol.com.br/>; accessed on 15 August 2023) online tool integrates several quantitative structures–activity relationship (QSAR) models by using the adverse outcome pathway (AOP) as a conceptual framework. The Organization for Economic Co-operation and Development (OECD) outlined the skin sensitization AOP framework with four key events (KE): KE1 is the covalent interaction of a substance with proteins present in the skin tested in direct peptide reactivity assay (DPRA); KE2 is epidermal keratinocytes activation tested in KeratinoSens assay; KE3 is dendritic cells activation tested in human cell line activation test (h-CLAT); and KE4 is proliferation of T-cells tested in murine local lymph node assay (LLNA) (OECD, 2014). Further, a consensus model was created by considering the average prediction of all models.

2.9.4. Modeling of molecular descriptors and biomarkers

To determine whether specific features of Si-QACs could induce a specific toxicological endpoint, a correlation between the categorization system of all endpoints and molecular descriptors of the synthesized Si-QACs was established.

A categorization system was generated to assess Si-QAC mutagenicity (SMART), genotoxicity (Comet-DSB), oxidative stress (OSI), cytotoxicity (indicated by trypan blue assay in the midgut), and apoptosis (caspases activities confirmed with apoptosis-related gene expressions) endpoints. If the experiment reported no significant statistical change, the Si-QAC was categorized as (1) nontoxic. In case one concentration reported a statistically significant change compared to the negative control, or a linear concentration-response relationship was observed, the Si-QAC was considered as (2) slightly toxic. Two or more concentrations displaying significant changes compared to the negative control, or one concentration reported a statistically significant change compared to the negative control with a linear concentration-response relationship, the Si-QAC was considered as (3) toxic.

The same approach was used for neurotoxicity assays (pupal position, negative geotaxis, crawling, climbing, thermal, and cold sensitivity assays). Each test received a score (1, no change; 2, one concentration-reported change/linear concentration-response; and 3, two or more concentrations presented change/one concentration-reported change with linear concentration-response). Subsequently, a cumulative scoring system was established to assess neurotoxicity. Si-QACs were categorized as (1) non-neurotoxic, (2) slightly neurotoxic, or (3) neurotoxic according to cumulative scores of 0–5, 6–10, and 11–15, respectively.

The DNA repair efficiency endpoint (RT²-PCR) was subjected to clustering analysis. If both concentrations (25% and 300%) of the same Si-QAC upregulated nearly all genes and were present in the same cluster, the Si-QAC was categorized as (1) nontoxic. If one concentration was upregulated and the other downregulated almost all genes, and each concentration was presented in a different cluster, the Si-QAC was categorized as (2) slightly toxic. If both concentrations of the same Si-QAC downregulated most of the genes and were present in the same cluster, Si-QAC was categorized as (3) toxic.

A descriptor list (nearly 5700 in number) was compiled from the OCHEM database [56], redundant variables with (i) a constant or nearly constant value, (ii) low variance (threshold=0.1), and (iii), values with correlation above 0.9 were omitted from this list.

A principal component analysis (PCA) was performed to understand the correlation between the Si-QAC descriptors and the observed toxicological endpoints, based on the score of each assay. Assays with the same score for all Si-QACs were excluded from the analysis. Descriptors and toxicological endpoints were selected as variables (n = 9). The number of principal components was selected based on the cumulative variation.

2.10. Statistical analysis

Statistical analysis of the SMART assay was conducted using MICROSTA software following the multiple-decision procedure [17] and the conditional binomial test with a probability level set at 0.05 [29]. The remaining assays were analyzed using SPSS software (version 20, IBM, Armonk, NY, USA) following one-way ANOVA and post hoc Dunnett test. PCA analysis was performed using RStudio (version 2022.12.0 +353).

3. Results and discussion

3.1. Si-QACs characterization

Various Si-QACs with different alkyl chain lengths (12, 14, 16, and 18 C atoms) and different structures were synthesized via the reaction of the silane group (Fig. 1). All synthesized compounds were obtained with $\geq 99.5\%$ purity (as determined by elemental analysis) and satisfactory yields (Table 2). The structures of all compounds were confirmed by FT-IR spectroscopy (Fig. S1, Supplementary Materials).

It is crucial to note that alcohol costs less per kilogram as an active disinfectant than the Si-QACs synthesized in this study. However, the amount of alcohol used in disinfectant formulations is considerably high (e.g., 60% v/v), whereas the concentration of Si-QACs in disinfectants is low (<1% v/v) [51]. Moreover, repeated and long-term use of alcohol-based disinfectants causes skin irritation and dryness. They are flammable products that require special storage and transportation conditions, making Si-QAC-based water-borne formulations attractive in terms of cost-effectiveness [5].

3.2. Antimicrobial activities

The synthesized disinfectants comprised QAC structures with various alkyl chain lengths (C12, C14, C16, and C18) and a counterion (silane). Initially, the effect of the dimethyl group (i.e., the alkyl group) on antimicrobial activity was assessed. A chain length of C16 was selected because its intermediate length balances the advantages associated with shorter and longer alkyl chains. Si-QAC-3 (with a dimethyl group, C16) had a lower MIC value against all tested bacteria than Si-QAC-4 (without a dimethyl group, C16). Thus, the absence of the dimethyl group reduced the antimicrobial potential of Si-QAC. According to the MIC results, Si-QAC-1 (C12) and Si-QAC-2 (C14) showed greater antimicrobial activity against Gram-positive bacteria than against Gram-negative bacteria (Table S3). In contrast, Si-QAC-3 (C16), Si-QAC-4 (C16), and Si-QAC-5 (C18) were more effective against Gram-positive bacteria. Thus, the short alkyl chain showed low antibacterial activity toward Gram-negative bacteria owing to the presence of the outer membrane and lipopolysaccharide, preventing entry into the plasma membrane. This finding was consistent with that of a previous study [7]. Furthermore, the antimicrobial activity of QAC was enhanced by the counterion, silane.

Disinfectant resistance can occur through mutational alterations in target affinity, efflux pump expression, and the acquisition of resistance-conferring genes [59]. For example, mono-QACs display high MIC values against efflux gene-carrying strains, such as *E. coli* and *P. aeruginosa* [41]. In the current study, a large difference in the MIC between QACs and Si-QACs was observed. The higher MIC results for QACs compared to Si-QACs could also be related to reducing the killing efficiency of these disinfectants [68]. This suggests that the Si-QACs are less prone to bacterial resistance. It is worth mentioning that the development of resistance depends on the concentration, physical state of the disinfectant, and environmental factors, including temperature. Thus, replacing existing disinfectants with the recommended concentrations of newly synthesized disinfectants can minimize the risk of resistance development [59].

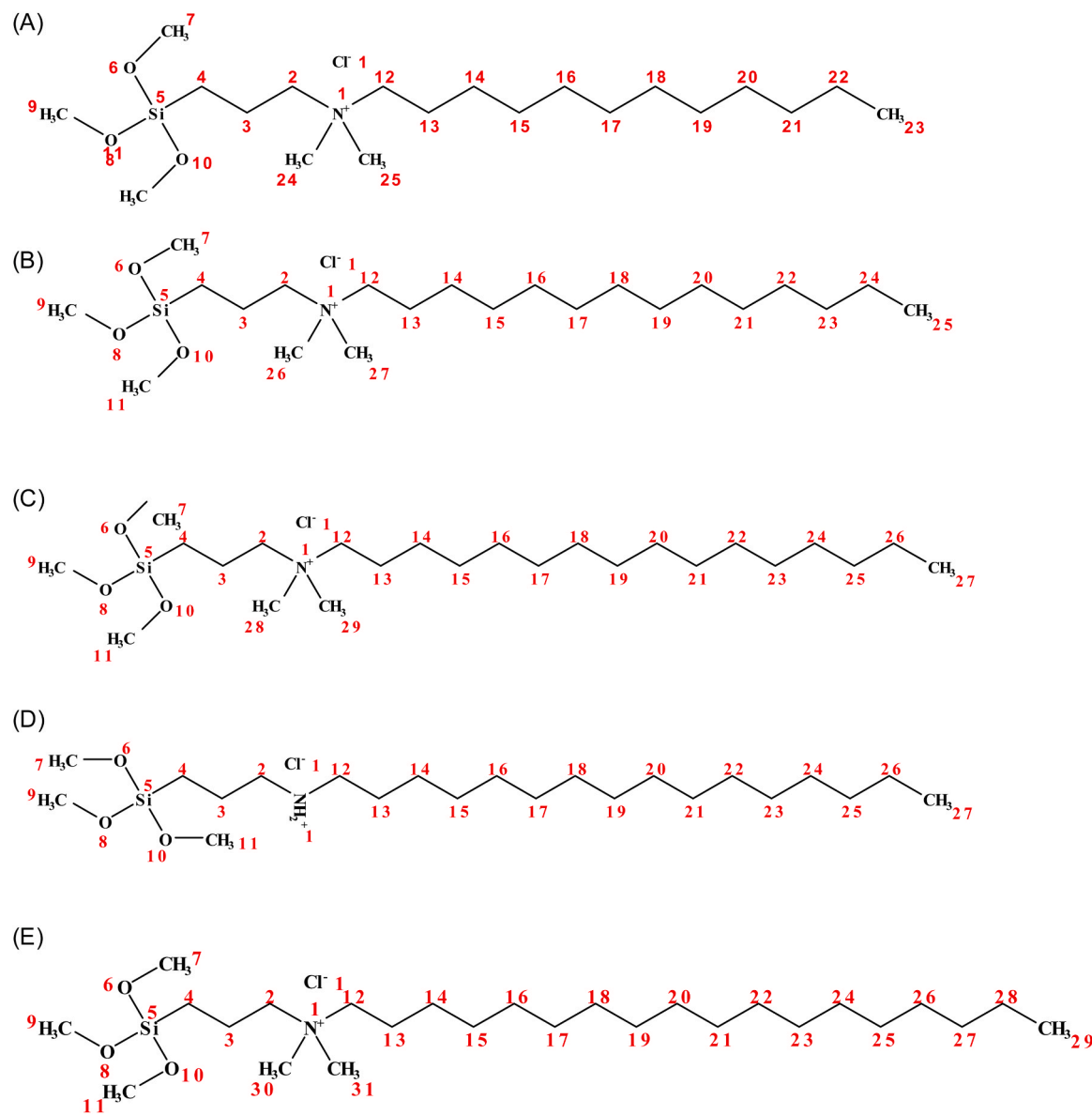


Fig. 1. 2D structures of Si-QACs. (A) Si-QAC-1, (B) Si-QAC-2, (C) Si-QAC-3, (D) Si-QAC-4, and Si-QAC-5.

Table 2
Yields of the synthesized Si-QACs.

Code	Chain	Name	Yield (%)
Si-QAC-1	C12	Dimethyldodecyl[3-(trimethoxysilyl)propyl] ammonium chloride	88.0
Si-QAC-2	C14	Dimethyltetradecyl[3-(trimethoxysilyl)propyl] ammonium chloride	85.3
Si-QAC-3	C16	Dimethylhexadecyl[3-(trimethoxysilyl)propyl] ammonium chloride	90.0
Si-QAC-4	C16	Hexadecyl[3-(trimethoxysilyl)propyl]ammonium chloride	98.5
Si-QAC-5	C18	Dimethyloctadecyl[3-(trimethoxysilyl)propyl] ammonium chloride	80.4

3.3. Biomarkers

D. melanogaster is an excellent model organism that is frequently used in various fields of biomedical research, including genotoxicity [42], antigenotoxicity [3], and neurotoxicity [9]. It shares nearly 80% of its identity in functional protein domains with humans, and 75% of human disease-related genes have homologs in *Drosophila* [45]. Furthermore, *Drosophila* exhibits a powerful detoxification process and DNA repair system like those in humans [40,55]. In our study, *Drosophila* flies were initially exposed to five different Si-QACs (at five different concentrations) via food intake throughout the larval stage to establish a reference set of exposure concentration ranges for further experiments. No lethal concentrations (LC_{50}) of these Si-QACs were detected (Fig. S2). Thus, all tested concentrations (25%, 50%, 100%, 200%, and 300%) were selected for the subsequent assays.

3.3.1. Mutagenicity and genotoxicity

Exposure to Si-QAC-1 at all concentrations (25%, 50%, 100%, 200%, and 300%) induced an increase in the frequency of total spots, *mwh* spots (mutational events or mitotic recombination), as well as small single

spots (mutational events or mitotic recombination), but inconclusive results were recorded for twin spots (mitotic recombination). Thus, Si-QAC-1 exerts mutagenic effects on *Drosophila*. Similarly, only a high concentration of Si-QAC-2 (300%) caused an increase in the frequency of the total spots, *mwh* spots, and small single spots. The frequency of mutant spots did not differ between the negative control and the remaining Si-QAC-2 concentrations. These results suggest that Si-QAC-2 (300%) has a weak mutagenic potential. Exposure to Si-QAC-3, - 4, and - 5 did not cause mutagenic or recombinogenic damage at any tested concentrations. The results are summarized in [Table S4](#).

On the other side, an increase in tail intensity was observed in larvae exposed to Si-QAC-1 (100%), Si-QAC-3 (25%, 50%, 100%, and 200%), Si-QAC-4 (50%, 200%, and 300%), and Si-QAC-5 (50%, 100%, 200%, and 300%) compared to unexposed larvae ([Fig. 2](#)). Remarkably, no DSB was reported in larvae exposed to Si-QAC-2.

According to our findings from the two well-established assays, SMART (mutation and recombination endpoints) and comet (DSB), the mutagenic potential recorded after exposure to Si-QAC-2 (300%) was probably associated with an event distinct from DSB induction. In contrast, an increase in DSB has been reported in larvae exposed to Si-QAC-3, - 4, and - 5, and no mutagenic effects have been observed. DSB may trigger the DNA repair process, impeding mutations that can be expressed in the phenotype [\[10\]](#). Si-QAC-1 exhibited mutagenic effects, but only 100% concentration increased DSB, which could be related to hormesis, where the lowest and highest concentrations reported no observed adverse effects compared to the intermediate concentrations [\[38\]](#).

3.3.2. Cytotoxicity

The trypan blue assay allows the assessment of cytotoxicity in *Drosophila* midgut cells according to the presence of blue staining inside the larvae ([Fig. S3](#)).

When the effects were quantified, moderate damage to the midgut of larvae exposed to Si-QAC-3 (300%) was observed, whereas major damage was observed in larvae exposed to Si-QAC-1 (200% and 300%), Si-QAC-3 (100% and 200%), and Si-QAC-4 (100% and 200%). Only Si-QAC-5 (300%) induced extreme damage to the larval midgut ([Fig. 3](#)). Interestingly, there was no record of midgut damage in larvae exposed to Si-QAC-2. Overall, several degrees of damage were observed in Si-QAC-1, - 3, - 4, and - 5, particularly at the highest concentrations. The induction of DNA damage and cell cycle perturbations with DNA repair deficiency can lead to cytotoxicity [\[53\]](#).

3.3.3. Apoptosis

The activated caspase 3/7 (Drice), 8 (Dredd), and 9 (Dronc) levels were subjected to increase after exposure to all Si-QACs at all concentrations, except for the caspase 3/7 level in larvae exposed to Si-QAC-1 (50%) ([Fig. S4](#)). These results imply the potential activation of the apoptotic mechanism. However, the multiple functions of caspases in *Drosophila* elicit a critical reconsideration of the proposed apoptotic mechanism. For instance, Drice plays a key role as a regulator of inflammatory signaling by interacting with *Drosophila* iap2 (Iap2) [\[32\]](#). Furthermore, Dredd functions as a regulator of the inflammatory response triggered by Gram-negative bacteria [\[34\]](#). It is worth noting that cells induce caspase activation in response to oxidative stress and/or inflammation to perform certain biological functions, such as the removal of damaged organelles through a process named 'restricted apoptosis' or 'non-lethal caspase activation' [\[26\]](#).

It is important to note that some of the genes studied in our RT²-PCR panel, such as *CdK7* and *p53*, play crucial roles in apoptosis signaling; however, these genes have several functions beyond apoptosis. By scrutinizing our RT²-PCR panel, the *Sirt2* gene was found to be involved in various cellular responses, including apoptosis signaling, as an anti-apoptotic gene. No change has been recorded in *Sirt2* gene expressions in larvae exposed to Si-QAC-4 (300%) or Si-QAC-5 (300%). On the other hand, upregulation in *Sirt2* gene expression in larvae exposed to Si-QAC-1 (25%) and Si-QAC-3 (300%) has been observed whereas down-regulation in the expressions of the same gene has been reported in larvae exposed to Si-QAC-1 (300%), Si-QAC-2 (25%, 300%), Si-QAC-3 (25%), Si-QAC-4 (25%), and Si-QAC-5 (25%). These findings suggest that caspase activation may not depend solely on apoptosis but also on oxidative stress.

3.3.4. Oxidative stress

The TOS levels increased in all Si-QACs, whereas the TAS levels decreased ([Fig. S5](#)). Hence, the oxidative stress index (OSI) increased in larvae exposed to Si-QACs compared to that in unexposed larvae. Remarkably, the OSI level of larvae exposed to Si-QAC-2 was limited compared with that of the negative control. Likely, the DNA damage and caspase activation recorded in the Si-QACs were partially related to oxidative stress.

3.3.5. DNA damage

To comprehensively understand the mechanisms underlying different toxicological endpoints, a possible DNA repair deficiency was anticipated. An RT²-PCR DNA panel of 36 genes involved in the DNA

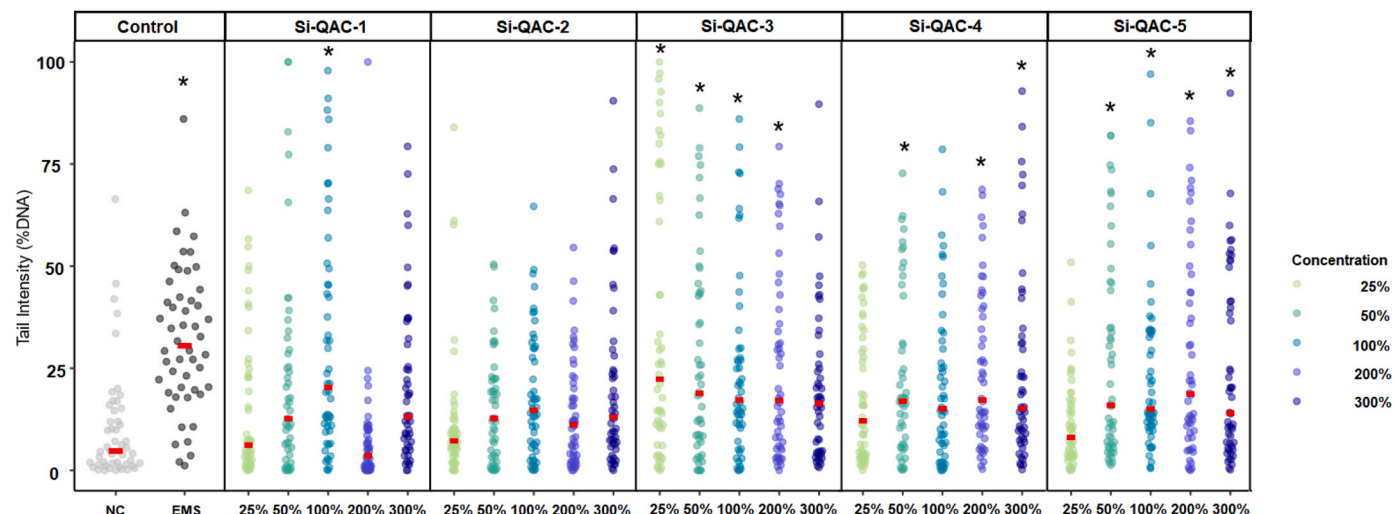


Fig. 2. Tail intensity in hemocytes of *Drosophila* larvae exposed to Si-QACs was assessed by the comet assay (single-cell gel electrophoresis). Fifty cells per treatment were analyzed. The short red line represents the median value. NC, negative control (distilled water); EMS (4 mM).

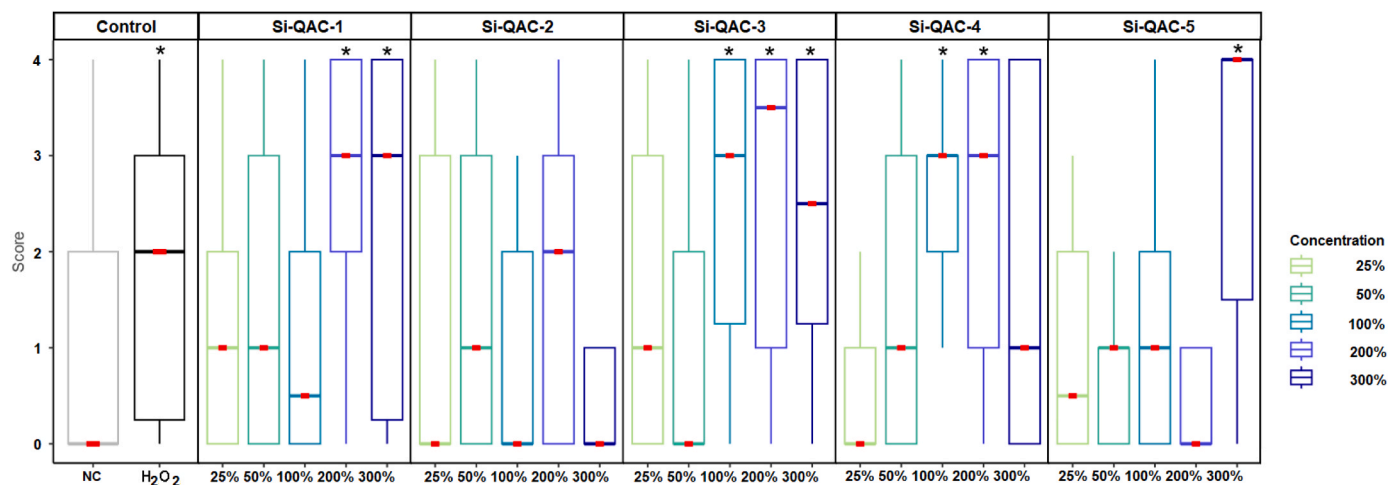


Fig. 3. Cell damage in the midgut of *Drosophila* larvae exposed to Si-QACs. Score values ((0) no blue color, no damage; (1) blue-colored dot, low damage; (2) two blue-colored dots, moderate damage; (3) approximately half of the midgut is blue-colored, major damage; and (4) blue-dark-colored midgut, extreme damage). The short red line represents the median value. NC, negative control (distilled water); H₂O₂ (0.05 M).

repair mechanism in *Drosophila*, selected based on human ortholog scores, was used (Table S5, *Supplementary Materials*). Two clusters have been identified: Si-QAC-2 (25%), Si-QAC-3 (300%), Si-QAC-4 (300%), and Si-QAC-3 (25%) were part of the same cluster (most genes were upregulated), and Si-QAC-1 (25% and 300%), Si-QAC-2 (300%), Si-QAC-4 (25%), Si-QAC-5 (25% and 300%) belong to the same cluster (majority of genes were downregulated) (Fig. 4; Table S6, *Supplementary Materials*). Under oxidative and genotoxic stress, DNA repair mechanisms trigger the upregulation of various genes that promote the repair of damaged DNA. However, if DNA damage exceeds the repair capacity, DNA repair genes may be downregulated due to feedback mechanisms or resource limitations. Furthermore, mutations can impede the expression of DNA repair genes by disrupting the transcription factor-binding sites [24].

Consequently, compounds belonging to the second cluster (Si-QAC-1 (25% and 300%), Si-QAC-2 (300%), Si-QAC-4 (25%), Si-QAC-5 (25% and 300%)- ‘downregulated cluster’) cause severe DNA damage compared to compounds from the first cluster (Si-QAC-2 (25%), Si-QAC-3 (25% and 300%), Si-QAC-4 (300%)-‘upregulated cluster’). Moreover, it is suggested that Si-QAC-1 (300%) causes more DNA damage compared to the other Si-QACs, owing to extensive downregulation of DNA repair gene expression.

In the first cluster, Si-QAC-2 (25%) induced the upregulation of gene expression involved in the DSB repair mechanism. Notably, there was no change in the expression of apoptosis- or NER-related genes. No significant changes were observed in the SMART and comet assays; however, an increase in caspase activity was reported. The upregulation of DSB-related genes is likely linked to cross-interactions between DNA repair pathways [43]. In contrast, high caspase levels and normal expression of apoptosis-related genes may be associated with cellular stress or dysfunction. In response to stress, cells activate survival pathways or initiate different cell death mechanisms [18]. As mentioned above, oxidative stress was recorded in larvae exposed to Si-QAC-2 (25%), thereby explaining the reason for caspase activation.

For Si-QAC-3 (300%), 35 genes were upregulated, and the expression of *Fancd2* remained unchanged. This suggests that all DNA repair mechanisms except the crosslinking repair mechanism were induced. However, no genotoxic effects were observed in the SMART and comet assays. Since DNA repair activation is likely induced by oxidative stress, such an effect may not be strong enough to be translated to genotoxicity, remarking the high sensitivity of determining DNA repair activation as a biomarker. The remaining Si-QACs did not follow specific DNA repair pathways.

3.3.6. Neurotoxicity

Drosophila larvae, with a complex nervous system, have emerged as a promising model system for studying the neuronal regulation of locomotion [25]. Crawling (99.8% forward vs. 0.2% backward) is a stereotypical behavior that occurs during larval foraging and in response to sensory stimuli, including temperature [62]. This locomotion pattern results from peristaltic contractions of the abdominal muscle segments (A1–A8) controlled by a chain of excitatory and inhibitory interneurons that promote wave propagation toward the desired destination. Notably, both the head and the thoracic segments (T1–T3) have distinct patterns of motion [22]. Only larvae exposed to Si-QAC-3 (300%) crawled a greater distance compared to unexposed larvae (Fig. 5). Thus, excitatory interneurons that support forward motion are affected.

Following the larval feeding stage, *Drosophila* larvae crawl to locate suitable sites for metamorphosis. The travel distance reveals the performance of the larval neuromuscular system [9]. Larvae exposed to Si-QAC-1 selected a position far from the medium compared to larvae exposed to the remaining Si-QACs and unexposed larvae (Fig. S6). Therefore, Si-QAC-1 possesses repellent properties.

The negative geotaxis or climbing assay has been used to assess age-related locomotor disorders. With age, the climbing speed declines, and the delay in starting to climb increases. Therefore, poor climbing performance is associated with neuromotor dysfunction (Dinter et al., 2016). Larvae exposed to Si-QACs exhibited good climbing performance; therefore, no neuromotor damage was observed (Fig. S7).

Nociception is a conserved defense mechanism in *Drosophila* that maintains homeostasis and minimizes tissue damage. Sensory neurons detect a potentially harmful stimulus, and the identification input triggers downstream pathways, yielding nocifensive responses to escape tissue-damaged stimuli [23]. *Drosophila* larvae require a warm temperature (24 °C) during the early larval stages, including the middle third larval stages, but a cooler temperature (18–20 °C) is needed at the end of the third larval stage [61]. Exposure to harmful temperatures activates a nocifensive escape locomotion response controlled by TRPA1 and painless channels [67]. However, harmful colds cause a bilateral contractile response, as detected by several ionotropic receptors. This response can be described as the compression of both the head and tail toward the midline of the larvae [60]. An increase in the number of larvae sensitive to harmful temperatures was observed after exposure to Si-QAC-1 (25%), Si-QAC-2 (25%, 50%, and 200%), and Si-QAC-3 (25%, 50%, 100%, 200%, and 300%) (Fig. 6).

On the other hand, larvae exposed to Si-QAC-1 and – 4 in cold sensitivity assay remained stationary, whereas larvae exposed to Si-QAC-2 (100%, 200%, and 300%), Si-QAC-3 (50%, 100%, 200%, and

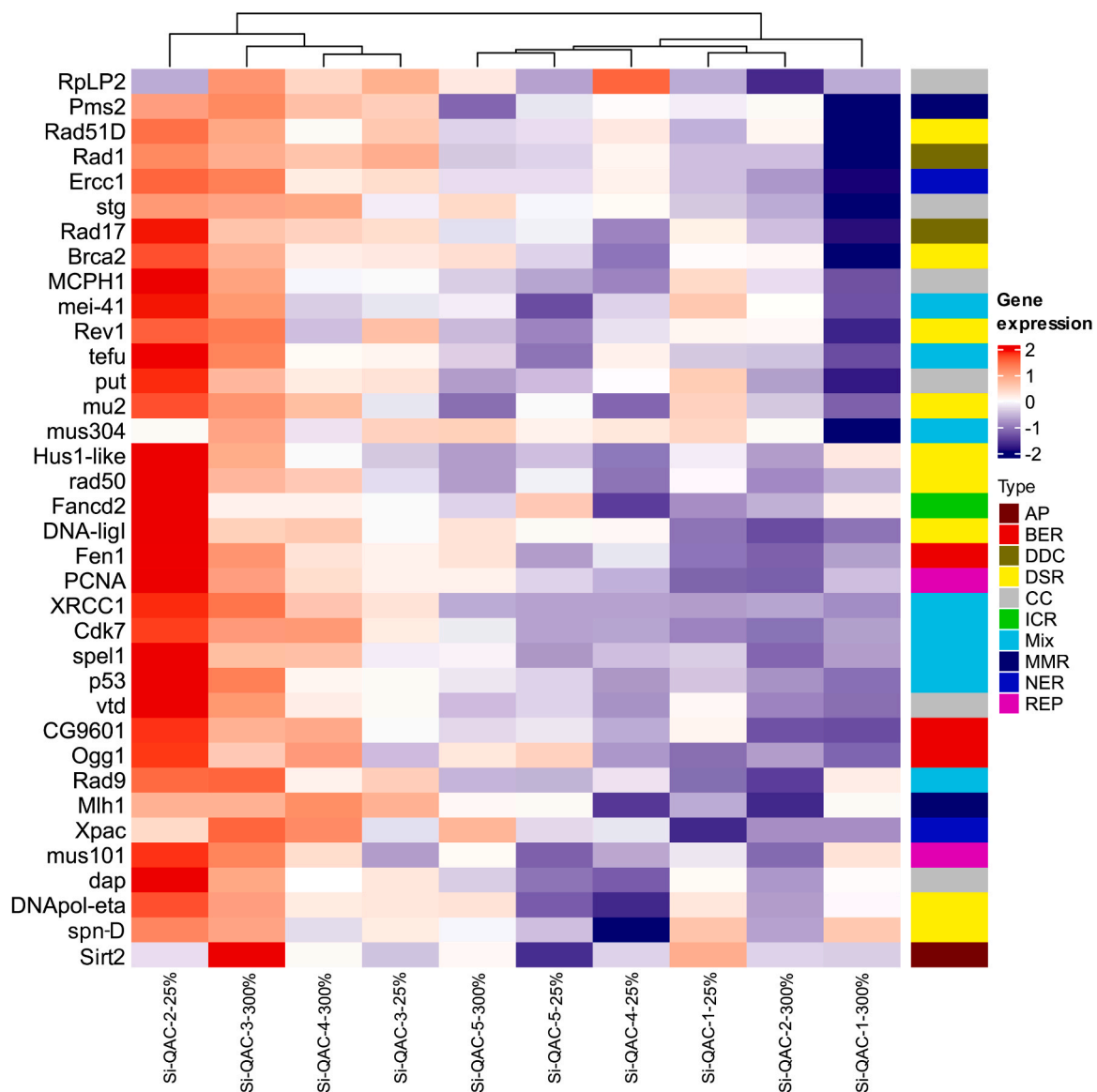


Fig. 4. A clustered heat map depicting the expression patterns in 36 DNA repair genes under Si-QACs exposure based on log2 fold change. Red denotes high expression, and blue low expression. The dendrogram shows two clusters stratified using hierarchical clustering. DNA repair gene's function was retrieved from FlyBase (<https://flybase.org/>; version FB2023_03, published on June 13, 2023). The biological process (gene ontology) is based on experimental evidence, and in the absence of experimental evidence, terms based on predictions or assertions have been selected. AP, Apoptosis; BER, Base excision repair; DDC, DNA damage checkpoint; DSR, Double strand breaks repair; CC, Cell cycle; ICR, Inter-crosslink repair; Mix, mixture (Details available in Table S6, Supplementary Materials); MMR, Mismatch repair; NER, Nucleotide excision repair; REP, DNA replication checkpoint.

300%), and Si-QAC-5 at all concentrations exhibited diminished mobility compared to negative control (Fig. S8).

3.4. *in silico* analysis

Si-QAC-1 had the best binding conformation with DNA (-13.70 kcal/mol), followed by Si-QAC-2 (Table S7, Supplementary Materials). As illustrated in Fig. S9, the interactions of Si-QAC-1 with DNA were generally Pi-alkyl, whereas van der Waals interactions dominated the interactions of Si-QAC-2 with DNA. The 3D structure and interactions between DNA and Si-QAC-2 are shown in Fig. 7(a, b). Colored arrows indicate the number of clusters that report the direction of motion of the DNA molecule. The deformability plots of the complexes are shown in Fig. 7c. The presence of hinges emphasizes the areas in the structure where the deformability is most pronounced. The B-factors (Fig. 7d) represent the degree of atomic movement around the balanced arrangement. Eigenvalues denote the concept of motion stiffness, which

is intricately linked to the amount of energy required to deform a structure. The lowest eigenvalue was observed for DNA-(Si-QAC-1), followed by DNA-(Si-QAC-2), indicating high stability (Fig. 7e; Fig. S10). The variance map (Fig. 7f) is inversely proportional to the eigenvalues. The covariance matrix is shown in Fig. 7g, illustrating the correlations between pairs of atoms (white, uncorrelated; red, correlated; blue, anti-correlated). The elastic network model (Fig. 7h) represents the relationship between the atoms (darker gray). The simulation results suggested that DNA-(SiQAC-2) was more stable than the other Si-QACs (Figs. S10, S11, S12, and S13). Shape-selective compounds generally bind to DNA through minor grooves [30]. This was similarly applied to Si-QACs as minor groove binders. Overall, DNA seems to be a target for Si-QAC activity and thus may be one of the reasons for DNA damage.

To understand the antiviral potential of Si-QACs, as a preliminary study, human adenovirus type 5 (HADV, Capsid protein hexon), SARS-CoV-2 (ACE-2), and influenza strain H5N1 (RdRp) were selected for

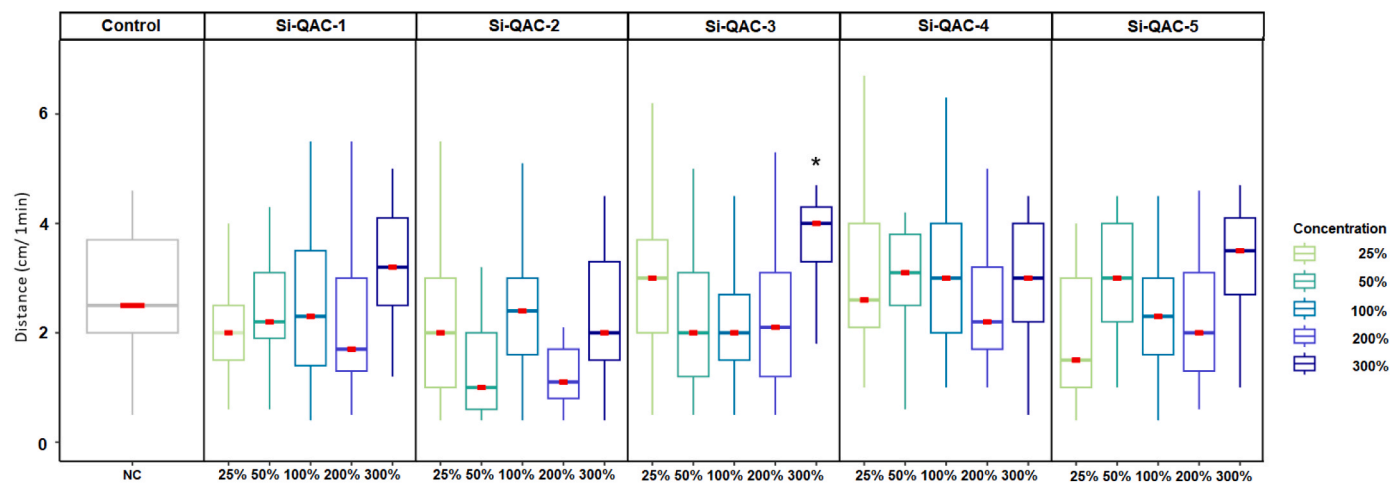


Fig. 5. Crawling distance of larvae under Si-QACs exposure. The short red line represents the median value. NC, negative control (distilled water), $n = 15$ per replica.

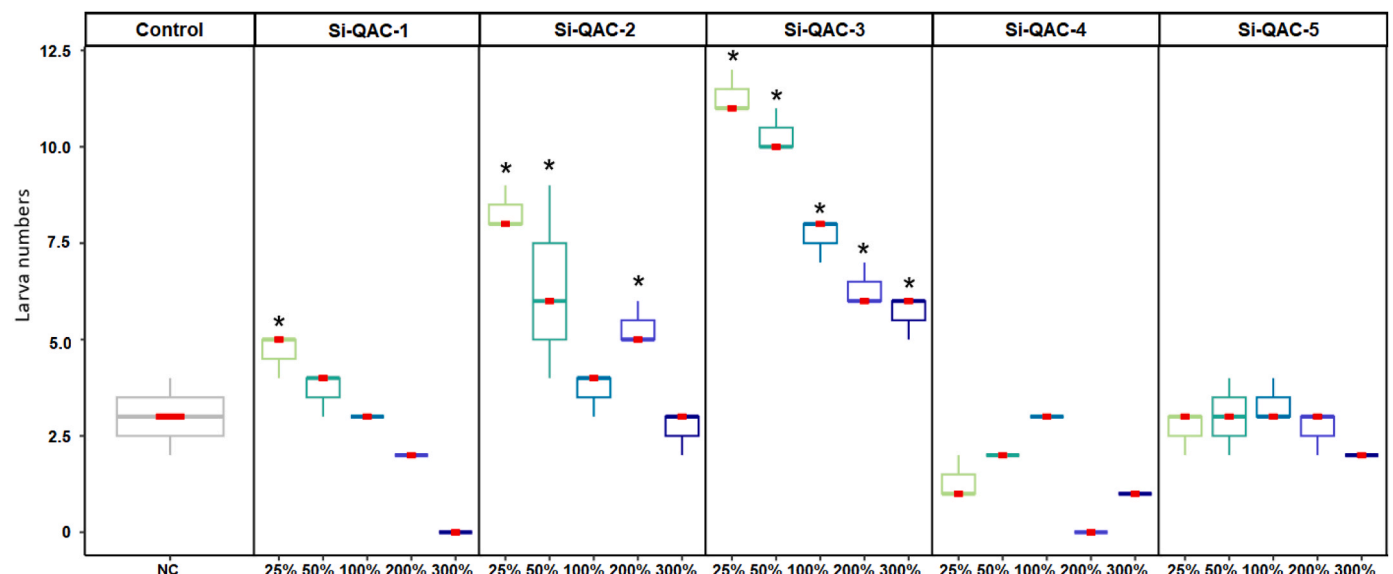


Fig. 6. Thermal sensitivity assay of larva exposed to Si-QACs. The red short-line represents the median value. NC, negative control (distilled water), $n = 15$ per replica.

molecular docking (Figs S14, S15, and S16). Adenovirus type 5 is a double-stranded, non-enveloped DNA virus associated with ocular, respiratory, and gastrointestinal disorders and can persist in humans in the latent state [48]. SARS-CoV-2 is responsible for the coronavirus disease (COVID-19) pandemic and has a strong affinity for ACE-2, which is expressed in several human organs [1]. The influenza strain H5N1 has emerged in recent years with a high mortality rate in humans and relies on RdRp as a crucial enzyme for viral replication [49]. Although the binding affinities of Si-QAC-5 against ACE-2, capsid hexon proteins, and RdRp were the most negative values compared to the remaining Si-QACs, suggesting a strong binding activity of the ligand, the binding interactions were unfavorable bumps, indicating unstable situations. As shown in Table S8, the binding energies of Si-QAC-1, -2, and -3 against ACE and HADV were related to the chain length of the Si-QACs; the longer the chain length, the stronger the binding activity. A prediction tool, Pred-Skin, was also used to predict skin sensitization. The results showed satisfactory confidence levels and predicted that all Si-QACs were non-sensitizers (Table S9). Notably, the concentrations of the tested Si-QACs were not considered.

In summary, although Si-QAC-2 ranked first against RdRp, second against hexon proteins, and third against ACE-2 in terms of antiviral potential based on in silico analysis, in vivo assays reported low to moderate toxicological outcomes compared to the remaining Si-QACs. Consequently, Si-QAC-2 was selected as the optimal disinfectant.

The retrieved descriptors are listed in Table S10. The first principal components (PC1 and PC2) accounted for 70.35% of the total variation. The PCA plot demonstrated that all variables were positively associated with PC1 except for "Mut" and "Panel," which both were positively associated with PC2 (Fig. 8).

The PCA plot demonstrated that all variables were positively associated with PC1 except for "Mut" and "Panel," which were both positively associated with PC2. Further, there is a positive correlation between genotoxicity (Gen), cytotoxicity (CYT), and the variables: "MW," "MoR07u," "Mor07s," and "LogP." Therefore, molecular weight, hydrophobicity/lipophilicity, and electron diffraction properties are crucial descriptors for guaranteeing the safety of Si-QAC.

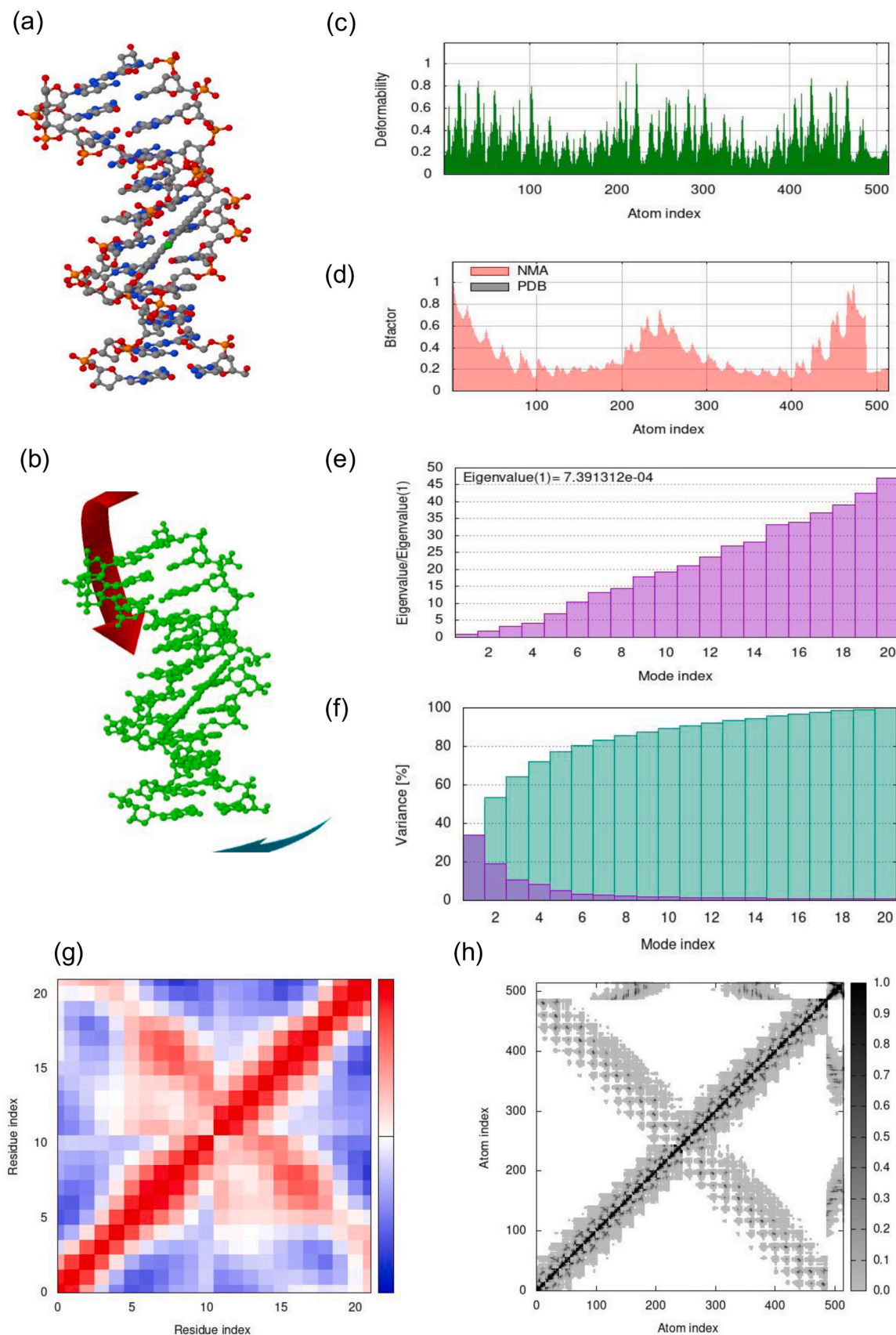


Fig. 7. 3D structure (a), interaction (b), deformability (c), B-factor (d), eigenvalue (e), variance map (f), covariance matrix (g), and elastic network (h) of NMA analysis by iMODS simulation of Si-QAC-2 with the DNA molecule. In the covariance matrix, colors denote the correlation between atoms (white, uncorrelated; red, correlated; blue, anti-correlated). In the elastic network, the intensity of the gray color is associated with the stiffness level. Dark gray dots indicate high stiffness springs.

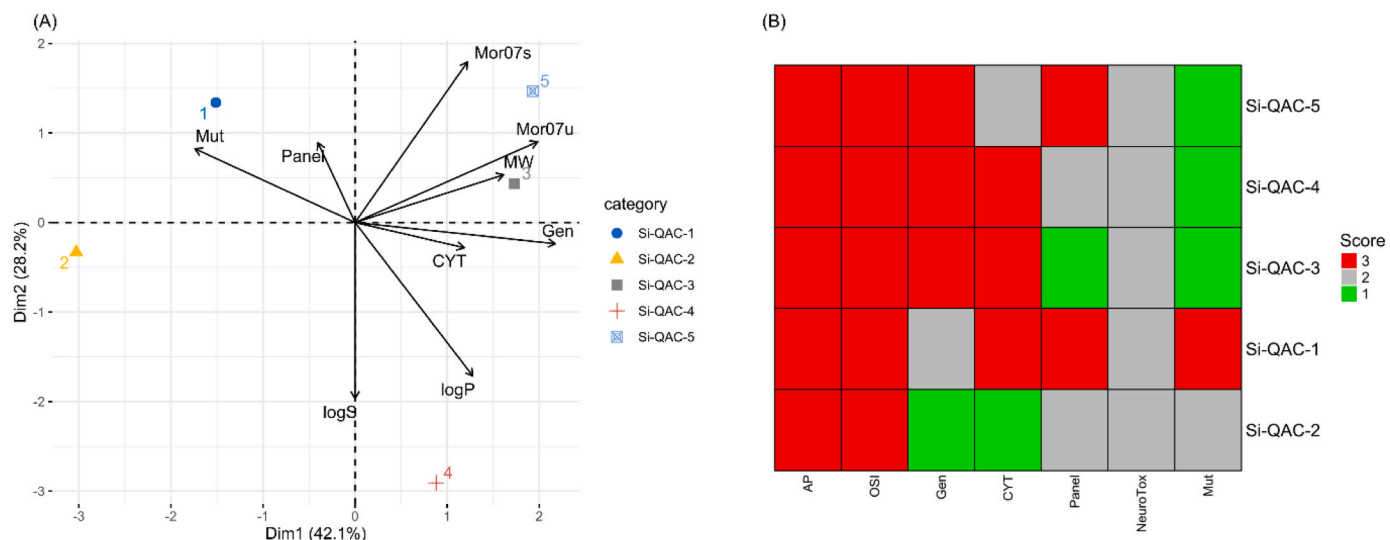


Fig. 8. Modeling of descriptors and toxicological endpoints. (A) PCA biplot of Si-QACs and variables. Narrow depicts the Mut, mutation score; Gen, comet score; CYT, cytotoxicity score; Panel, panel score. Dim1 and Dim2 Dimension, (B) Scores of each assay based on the categorization approach. AP, apoptosis; OSI, oxidative stress index; Gen, Genotoxicity (Comet); CYT, cytotoxicity (Trypan assay); NeuroTox, Neurotoxicity; Mut, Mutagenicity (SMART).

4. Conclusion

This study is an important step toward producing biocompatible disinfectants by synthesizing novel compounds (Si-QACs) and assessing their safety using *Drosophila* as an in vivo model organism, followed by in silico analysis. Si-QAC-2 reported moderate-to-low toxicological outcomes with high stability and anticipated strong antiviral potential compared with the remaining Si-QACs. However, additional research is required to explore the concentration-dependent effects of Si-QAC-2 on skin sensitivity. It is essential to acknowledge that extrapolating findings to diverse alternative organisms, including humans, remains a complex challenge. Although the used models predict the toxicity potential of Si-QACs, the obtained results do not necessarily guarantee a direct translation to other organisms.

Environmental implication

Disinfection products, such as quaternary ammonium compounds (QACs), are extensively used mainly because of the last pandemic. Due to the adverse health outcomes reported, they represent an environmental/health concern. In this context, biocompatible disinfectants with reduced side effects must be developed. This study has generated new compounds that, after a wide set of in vivo/in silico assays have obtained a future candidate covering safer environmental/health requirements.

Funding

This study was supported by the Scientific, Technological Research Council of Türkiye (TÜBİTAK) in the framework of the ARDEB 1001 Program [Grant No: 121Z809] and Akdeniz University Scientific Research Projects Coordination Unit [Grant No: FDK-2023-6161; Grant No: FYL-2021-5593].

CRediT authorship contribution statement

Kaya Nuray: Writing – review & editing. **Akarsu Esin:** Methodology. **Kaya Bülent:** Writing – review & editing. **Tagorti Ghada:** Data curation, Formal analysis, Methodology, Writing – review & editing. **Marcos Ricard:** Writing – review & editing. **Güneş Merve:** Methodology. **Yalçın Burçın:** Methodology. **Cihanoglu Neslihan:** Methodology. **Burgazlı Ayşen Yağmur:** Methodology. **Kuruca Tuğçe:** Methodology.

Declaration of Competing Interest

The authors declare that they have no known competing financial interests or personal relationships that could have appeared to influence the work reported in this paper.

Data availability

Data will be made available on request.

Acknowledgments

We would like to extend our gratitude to Prof. Dr. Sibel Tunç Laboratory (Chemistry Department, Akdeniz University) and Assoc. Prof. Dr. Esra Aydemir Laboratory (Biology Department, Akdeniz University) for generously providing access to the spectrometer and RT-PCR thermal cycler.

Appendix A. Supporting information

Supplementary data associated with this article can be found in the online version at [doi:10.1016/j.jhazmat.2024.133470](https://doi.org/10.1016/j.jhazmat.2024.133470).

References

- [1] Ali, F., Kasry, A., Amin, M., 2021. The new SARS-CoV-2 strain shows a stronger binding affinity to ACE2 due to N501Y mutant. *Med Drug Discov* 10, 100086. <https://doi.org/10.1016/j.medidd.2021.100086>.
- [2] Afshari, R., Akhavan, O., Hamblin, M.R., Varma, R.S., 2021. Review of oxygenation with nanobubbles: possible treatment for hypoxic COVID-19 patients. *ACS Appl Nano Mater* 4, 11386–11412. <https://doi.org/10.1021/acsnano.1c01907>.
- [3] Amliss, S., Dalouh, A., Idaomar, M., 2021. Chemical composition, genotoxicity and antigenotoxicity study of *Artemisia herba-alba* using the eye and wing SMART assay of *Drosophila melanogaster*. *Arab J Chem* 14, 102976. <https://doi.org/10.1016/j.arabjc.2020.102976>.
- [4] Arnold, W.A., Blum, A., Branyan, J., Bruton, T.A., Carignan, C.C., Cortopassi, G., et al., 2023. Quaternary ammonium compounds: a chemical class of emerging concern. *Environ Sci Technol* 57, 7645–7665. <https://doi.org/10.1021/acs.est.2c08244>.
- [5] Azelee, N.I.W., El-Enshasy, H., Joe Dailin, D., Abdul Manas, N.H., Abd Malek, R., Mokhter, M.A., et al., 2020. Antimicrobial disinfectants and sanitizers: an effective tool for breaking the circle of pandemic disease. *Asian J Agric Biol* 8, 348–367. <https://doi.org/10.35495/ajab.2020.06.355>.
- [6] Baty, F., Ritz, C., Charles, S., Brutsche, M., Flandrois, J.-P., Delignette-Muller, M.-L., 2015. A toolbox for nonlinear regression in R: the package nlstools. *J Stat Soft* 66 (5), 1–21. <https://doi.org/10.18637/jss.v066.i05>.

[7] Bazina, L., Maravić, A., Krce, L., Soldo, B., Odžak, R., Popović, V.B., et al., 2019. Discovery of novel quaternary ammonium compounds based on quinuclidine-3-ol as new potential antimicrobial candidates. *Eur J Med Chem* 163, 626–635. <https://doi.org/10.1016/j.ejmech.2018.12.023>.

[8] Boyce, J.M., 2023. Quaternary ammonium disinfectants and antiseptics: tolerance, resistance and potential impact on antibiotic resistance. *Antimicrob Resist Infect Control* 12, 32. <https://doi.org/10.1186/s13756-023-01241-z>.

[9] Cabrita, A., Medeiros, A.M., Pereira, T., Rodrigues, A.S., Kranendonk, M., Mendes, C.S., 2022. Motor dysfunction in *Drosophila melanogaster* as a biomarker for developmental neurotoxicity. *iScience* 25, 104541. <https://doi.org/10.1016/j.isci.2022.104541>.

[10] Chatterjee, N., Walker, G.C., 2017. Mechanisms of DNA damage, repair, and mutagenesis. *Environ Mol Mutagen* 58, 235–263. <https://doi.org/10.1002/em.22087>.

[11] Dhama, K., Patel, S.K., Kumar, R., Masand, R., Rana, J., Yatoo, Mohdi, et al., 2021. The role of disinfectants and sanitizers during COVID-19 pandemic: advantages and deleterious effects on humans and the environment. *Environ Sci Pollut Res* 28, 34211–34228. <https://doi.org/10.1007/s11356-021-14429-w>.

[12] Dhar, G., Mukherjee, S., Nayak, N., Sahu, S., Bag, J., Rout, R., et al., 2020. Various behavioural assays to detect the neuronal abnormality in flies. In: Mishra, M. (Ed.), *Fundamental Approaches to Screen Abnormalities in Drosophila*. Springer Protocols Handbooks. Springer US, New York, NY, pp. 223–251. https://doi.org/10.1007/978-1-4939-9756-5_18.

[13] Ebrahimi, M., Asadi, M., Akhavan, O., 2022. Graphene-based nanomaterials in fighting the most challenging viruses and immunogenic disorders. *ACS Biomater Sci Eng* 8, 54–81. <https://doi.org/10.1021/acsbiomaterials.1c01184>.

[14] Erel, O., 2005. A new automated colorimetric method for measuring total oxidant status. *Clin Biochem* 38, 1103–1111. <https://doi.org/10.1016/j.clinbiochem.2005.08.008>.

[15] Filipiak, M., Tylko, G., Pyza, E., 2012. Zinc induces caspase-dependent mitochondrial pathway of the programmed cell death in haemocytes of *Drosophila melanogaster*. *Biometals* 25, 507–516. <https://doi.org/10.1007/s10534-012-9530-1>.

[16] Frantz, A.L., 2023. Chronic quaternary ammonium compound exposure during the COVID-19 pandemic and the impact on human health. *Toxicol Environ Health Sci* 15, 199–206. <https://doi.org/10.1007/s13530-023-00173-w>.

[17] Frei, H., Würger, F.E., 1988. Statistical methods to decide whether mutagenicity test data from *Drosophila* assays indicate a positive, negative, or inconclusive result. *Mutat Res* 203, 297–308. [https://doi.org/10.1016/0165-1161\(88\)90019-2](https://doi.org/10.1016/0165-1161(88)90019-2).

[18] Fulda, S., Gorman, A.M., Hori, O., Samali, A., 2010. Cellular stress responses: cell survival and cell death. *Int J Cell Biol* 2010, 1–23. <https://doi.org/10.1155/2010/214074>.

[19] Gargano, J., Martin, I., Bhandari, P., Grotewiel, M., 2005. Rapid iterative negative geotaxis (RING): a new method for assessing age-related locomotor decline in. *Exp Gerontol* 40, 386–395. <https://doi.org/10.1016/j.exger.2005.02.005>.

[20] Gocke, E., Bürgin, H., Müller, L., Pfister, T., 2009. Literature review on the genotoxicity, reproductive toxicity, and carcinogenicity of ethyl methanesulfonate. *Toxicol Lett* 190, 254–265. <https://doi.org/10.1016/j.toxlet.2009.03.016>.

[21] Güneş, M., Yalçın, B., Burgazlı, E.Y., Tagorti, G., Yavuz, E., Akarsu, E., et al., 2023. Morphologically different hydroxyapatite nanoparticles exert differential genotoxic effects in *Drosophila*. *Sci Total Environ* 904, 166556. <https://doi.org/10.1016/j.scitotenv.2023.166556>.

[22] Heckscher, E.S., Lockery, S.R., Doe, C.Q., 2012. Characterization of *Drosophila* larval crawling at the level of organism, segment, and somatic body wall musculature. *J Neurosci* 32, 12460–12471. <https://doi.org/10.1523/JNEUROSCI.0222-12.2012>.

[23] Himmel, N.J., Letcher, J.M., Sakurai, A., Gray, T.R., Benson, M.N., Donaldson, K.J., et al., 2021. Identification of a neural basis for cold acclimation in *Drosophila* larvae. *iScience* 24, 102657. <https://doi.org/10.1016/j.isci.2021.102657>.

[24] Huang, R., Zhou, P.-K., 2021. DNA damage repair: historical perspectives, mechanistic pathways and clinical translation for targeted cancer therapy. *Signal Transduct, Target Ther* 6, 254. <https://doi.org/10.1038/s41392-021-00648-7>.

[25] Hunter, I., Coulson, B., Zarin, A.A., Baines, R.A., 2021. The *Drosophila* larval locomotor circuit provides a model to understand neural circuit development and function. *Front Neural Circuits* 15, 684969. <https://doi.org/10.3389/fncir.2021.684969>.

[26] Hyman, B.T., Yuan, J., 2012. Apoptotic and non-apoptotic roles of caspases in neuronal physiology and pathophysiology. *Nat Rev Neurosci* 13, 395–406. <https://doi.org/10.1038/nrn3228>.

[27] Irving, P., Ubeda, J.-M., Doucet, D., Troxler, L., Lagueux, M., Zachary, D., et al., 2005. New insights into *Drosophila* larval haemocyte functions through genome-wide analysis. *Cell Microbiol* 7, 335–350. <https://doi.org/10.1111/j.1462-5822.2004.00462.x>.

[28] Johnmark, N., Kinyi, H.W., 2021. Amaranth leaf extract protects against hydrogen peroxide induced oxidative stress in *Drosophila melanogaster*. *BMC Res Notes* 14, 188. <https://doi.org/10.1186/s13104-021-05603-x>.

[29] Kastenbaum, M.A., Bowman, K.O., 1970. Tables for determining the statistical significance of mutation frequencies. *Mutat Res* 9, 527–549. [https://doi.org/10.1016/0027-5107\(70\)90038-2](https://doi.org/10.1016/0027-5107(70)90038-2).

[30] Khan, G.S., Shah, A., Zia-ur-Rehman, Barker, D., 2012. Chemistry of DNA minor groove binding agents. *J Photochem Photobiol B: Biol* 115, 105–118. <https://doi.org/10.1016/j.jphotobiol.2012.07.003>.

[31] Kieslich, C.A., Alimirzaei, F., Song, H., Do, M., Hall, P., 2021. Data-driven prediction of antiviral peptides based on periodicities of amino acid properties. *Computer Aided Chemical Engineering*. Elsevier, pp. 2019–2024. <https://doi.org/10.1016/B978-0-323-88506-5.50312-0>.

[32] Kietz, C., Mohan, A.K., Pollari, V., Tuominen, I.-E., Ribeiro, P.S., Meier, P., et al., 2022. Drice restrains Diap2-mediated inflammatory signalling and intestinal inflammation. *Cell Death Differ* 29, 28–39. <https://doi.org/10.1038/s41418-021-00832-w>.

[33] Kula, N., Lamch, Ł., Futoma-Kołoch, B., Wilk, K.A., Obłak, E., 2022. The effectiveness of newly synthesized quaternary ammonium salts differing in chain length and type of counterion against priority human pathogens. *Sci Rep* 12, 21799. <https://doi.org/10.1038/s41598-022-24760-y>.

[34] Leulier, F., Rodriguez, A., Khush, R.S., Abrams, J.M., Lemaitre, B., 2000. The *Drosophila* caspase Dredd is required to resist gram-negative bacterial infection. *EMBO Rep* 1, 353–358. <https://doi.org/10.1093/embo-reports/kvd073>.

[35] López-Blanco, J.R., Aliaga, J.I., Quintana-Ortí, E.S., Chacón, P., 2014. iMODS: internal coordinates normal mode analysis server. *Nucleic Acids Res* 42, W271–W276. <https://doi.org/10.1093/nar/gku339>.

[36] Maghsoudi, S., Taghavi Shahraki, B., Rameh, F., Nazarabi, M., Fatahi, Y., Akhavan, O., et al., 2022. A review on computer-aided chemogenomics and drug repositioning for rational COVID-19 drug discovery. *Chem Biol Drug Des* 100, 699–721. <https://doi.org/10.1111/cbdd.14136>.

[37] Marcos R., Carmona E.R. 2019. The wing-spot and the comet tests as useful assays detecting genotoxicity in *Drosophila*. In: *Genotoxicity Assessment: Methods and Protocols*, Methods in Molecular Biology, A. Dhawan and M. Bajpayee (Eds.), Springer Science+Business Media, LLC, part of Springer Nature. Vol- 2031, Chapter 19, pp. 337–380.

[38] Mattson, M.P., 2008. Hormesis defined. *Ageing Res Rev* 7, 1–7. <https://doi.org/10.1016/j.arr.2007.08.007>.

[39] Mishra, M., Barik, B.K., 2018. Behavioral teratogenesis in *Drosophila melanogaster*. In: Félix, L. (Ed.), *Teratogenicity Testing, Methods in Molecular Biology*. Springer New York, New York, NY, pp. 277–298. https://doi.org/10.1007/978-1-4939-7883-0_14.

[40] Moraes, K.C.M., Montagne, J., 2021. *Drosophila melanogaster*: a powerful tiny animal model for the study of metabolic hepatic diseases. *Front Physiol* 12, 728407. <https://doi.org/10.3389/fphys.2021.728407>.

[41] Morrison, K.R., Allen, R.A., Minbøle, K.P.C., Wuest, W.M., 2019. More QACs, more questions: recent advances in structure activity relationships and hurdles in understanding resistance mechanisms. *Tetrahedron Lett* 60, 150935. <https://doi.org/10.1016/j.tetlet.2019.07.026>.

[42] Nesterkina, M., Bilonok, S., Alikseieva, T., Kravchenko, I., Hirsch, A.K.H., 2023. Genotoxic and mutational potential of monocyclic terpenoids (carvacrol, carvone and thymol) in *Drosophila melanogaster*. *Toxicol Rep* 10, 327–333. <https://doi.org/10.1016/j.toxrep.2023.02.009>.

[43] Oh, J.-M., Myung, K., 2022. Crosstalk between different DNA repair pathways for DNA double strand break repairs. *Mutat Res/Genet Toxicol Environ Mutagen* 873, 503438. <https://doi.org/10.1016/j.mrgentox.2021.503438>.

[44] Osimitz, T.G., Droege, W., 2022. Adverse outcome pathway for antimicrobial quaternary ammonium compounds. *J Toxicol Environ Health, P* A 85 (12), 494–510. <https://doi.org/10.1080/25287394.2022.2037479>.

[45] Pandey, U.B., Nichols, C.D., 2011. Human disease models in *Drosophila melanogaster* and the role of the fly in therapeutic drug discovery. *Pharmacol Rev* 63, 411–436. <https://doi.org/10.1124/pr.110.003293>.

[46] Pati, S.G., Arnold, W.A., 2020. Comprehensive screening of quaternary ammonium surfactants and ionic liquids in wastewater effluents and lake sediments. *Environ Sci: Proces Impacts* 22, 430–441. <https://doi.org/10.1039/C9EM00554D>.

[47] Peyneau, M., de Chaisemartin, L., Gigant, N., Chollet-Martin, S., Kerdine-Römer, S., 2022. Quaternary ammonium compounds in hypersensitivity reactions. *Front Toxicol* 4, 973680. <https://doi.org/10.3389/tox.2022.973680>.

[48] Pfitzner, S., Bosse, J.B., Hofmann-Sieber, H., Flomm, F., Reimer, R., Dobner, T., et al., 2021. Human adenovirus type 5 infection leads to nuclear envelope destabilization and membrane permeability independently of adenovirus death protein. *IJMS* 22, 13034. <https://doi.org/10.3390/ijms222313034>.

[49] Picarazzi, F., Vicenti, I., Saladini, F., Zazzi, M., Mori, M., 2020. Targeting the RdRp of emerging RNA viruses: the structure-based drug design challenge. *Molecules* 25, 5695. <https://doi.org/10.3390/molecules25235695>.

[50] Rad, M., Ebrahimpour, G., Bandehpour, M., Akhavan, O., Yarian, F., 2023. SOEing PCR/docking optimization of protein A-G/scFv-Fc-bioconjugated Au nanoparticles for interaction with meningitis bacterial antigen. *Catalysts* 13, 790. <https://doi.org/10.3390/catal13050790>.

[51] Ribeiro, M.M., Neumann, V.A., Padoveze, M.C., Graziano, K.U., 2015. Efficacy and effectiveness of alcohol in the disinfection of semi-critical materials: a systematic review. *Rev Lat-Am Enferm* 23, 741–752. <https://doi.org/10.1590/0104-1169.0266.2611>.

[52] RStudio Team. 2022. RStudio: Integrated Development for R. RStudio, PBC, Boston, MA URL <http://www.rstudio.com/>.

[53] Salih Istifli, E., Tahir Hüsunet, M., Basri Ila, H. 2019. Cell division, cytotoxicity, and the assays used in the detection of cytotoxicity, in: Salih Istifli, E., Basri Ila, H. (Eds.), *Cytotoxicity - Definition, Identification, and Cytotoxic Compounds*. IntechOpen. <https://doi.org/10.5772/intechopen.88368>.

[54] Sandhaus, S., Chapagain, P.P., Tse-Dinh, Y.-C., 2018. Discovery of novel bacterial topoisomerase I inhibitors by use of *in silico* docking and *in vitro* assays. *Sci Rep* 8, 1437. <https://doi.org/10.1038/s41598-018-19944-4>.

[55] Sekelsky, J., 2017. DNA repair in *Drosophila*: mutagens, models, and missing genes. *Genetics* 205, 471–490. <https://doi.org/10.1534/genetics.116.186759>.

[56] Sushko, I., Novotarskyi, S., Körner, R., Pandey, A.K., Rupp, M., Teetz, W., et al., 2011. Online chemical modeling environment (OCHEM): web platform for data storage, model development and publishing of chemical information. *J Comput Aided Mol Des* 25, 533–554. <https://doi.org/10.1007/s10822-011-9440-2>.

[57] Tagorti, G., Kaya, B. 2022. Publication trends of somatic mutation and recombination tests research: a bibliometric analysis (1984—2020). *Genomics Inform.* 20, e10. <https://doi.org/10.5808/gi.21083>.

[58] Tagorti, G., Yalçın, B., Güneş, M., Burgazlı, A.Y., Kaya, B., 2023. Comparative evaluation of natural and artificial sweeteners from DNA damage, oxidative stress, apoptosis, to development using *Drosophila melanogaster*. *Drug Chem Toxicol* 1–12. <https://doi.org/10.1080/01480545.2023.2228522> (Online ahead of print).

[59] Tong, C., Hu, H., Chen, G., Li, Z., Li, A., Zhang, J., 2021. Disinfectant resistance in bacteria: mechanisms, spread, and resolution strategies. *Environ Res* 195, 110897. <https://doi.org/10.1016/j.envres.2021.110897>.

[60] Turner, H.N., Armengol, K., Patel, A.A., Himmel, N.J., Sullivan, L., Iyer, S.C., et al., 2016. The TRP channels Pkd2, NompC, and Trpm Act in cold-sensing neurons to mediate unique aversive behaviors to noxious cold in *Drosophila*. *Curr Biol* 26, 3116–3128. <https://doi.org/10.1016/j.cub.2016.09.038>.

[61] Tyrrell, J.J., Wilbourne, J.T., Omelchenko, A.A., Yoon, J., Ni, L., 2021. Ionotropic receptor-dependent cool cells control the transition of temperature preference in *Drosophila* larvae. *PLOS Genet* 17, e1009499. <https://doi.org/10.1371/journal.pgen.1009499>.

[62] Wosniack, M.E., Festa, D., Hu, N., Gjorgjieva, J., Berni, J., 2022. Adaptation of *Drosophila* larva foraging in response to changes in food resources. *eLife* 11, e75826. <https://doi.org/10.7554/eLife.75826>.

[63] Xiao, S., Yuan, Z., Huang, Y., 2022. Disinfectants against SARS-CoV-2: a review. *Viruses* 14, 1721. <https://doi.org/10.3390/v14081721>.

[64] Xie, M., Gao, M., Yun, Y., Malmsten, M., Rotello, V.M., Zboril, R., et al., 2023. Antibacterial nanomaterials: mechanisms, impacts on antimicrobial resistance and design principles. *Angew Chem Int Ed* 62, e202217345. <https://doi.org/10.1002/anie.202217345>.

[65] Yalçın, B., Güneş, M., Kurşun, A.Y., Kaya, N., Marcos, R., Kaya, B., 2022. Genotoxic hazard assessment of cerium oxide and magnesium oxide nanoparticles in *Drosophila*. *Nanotoxicology* 16, 393–407. <https://doi.org/10.1080/17435390.2022.2098072>.

[66] Zheng, G., Filippelli, G.M., Salamova, A., 2020. Increased indoor exposure to commonly used disinfectants during the COVID-19 pandemic. *Environ Sci Technol Lett* 7, 760–765. <https://doi.org/10.1021/acs.estlett.0c00587>.

[67] Zhong, L., Bellemer, A., Yan, H., Honjo, K., Robertson, J., Hwang, R.Y., et al., 2012. Thermosensory and nonthermosensory isoforms of *Drosophila melanogaster* TRPA1 reveal heat-sensor domains of a ThermoTRP channel. *Cell Rep* 1, 43–55. <https://doi.org/10.1016/j.celrep.2011.11.002>.

[68] Zhu, Z., Shan, L., Zhang, X., Hu, F., Zhong, D., Yuan, Y., et al., 2021. Effects of bacterial community composition and structure in drinking water distribution systems on biofilm formation and chlorine resistance. *Chemosphere* 264, 128410. <https://doi.org/10.1016/j.chemosphere.2020.128410>.